2.34 EFFECT OF TRIPLE ION BEAM IRRADIATION ON MECHANICAL PROPERTIES OF HIGH CHROMIUM AUSTENITIC STAINLESS STEEL

Ikuo Ioka[1]*, Masatoshi Futakawa[1], Yoshiyasu Nanjyo[1], Kiyoshi Kiuchi[1], Yuji Kuroda[2] and Takefumi Anegawa[3]

[1]Japan Atomic Energy Research Institute, Department of Nuclear Energy System
2-4 Shirakata Shirane, Tokai-mura, Ibaraki-ken, 319-1195 Japan
[2]The Japan Atomic Power Company, , Research and Development Department
6-1, 1-chome, Ohtemachi, Chiyoda-ku, Tokyo, 100-0004 Japan
[3]Tokyo Electric Power Company, Nuclear Power Engineering Department
1-3 Uchisaiwai-cho, 1-choume, Chiyoda-ku, Tokyo, 100-0011 Japan

Abstract

A high-chromium austenitic stainless steel has been developed for an advanced fuel cladding tube considering waterside corrosion and irradiation embrittlement. The candidate material was irradiated in triple ion (Ni, He, H) beam modes at 573K up to 50dpa to simulate irradiation damage by neutron and transmutation product. The change in hardness of the very shallow surface layer of the irradiated specimen was estimated from the slope of load/depth-depth curve which is in direct proportion to the apparent hardness of the specimen. Besides, the Swift's power low constitutive equation ($\sigma=A(\varepsilon_0+\varepsilon)^n$, A: strength coefficient, ε_0: equivalent strain by cold rolling, n: strain hardening exponent) of the damaged parts was derived from the indentation test combined with an inverse analysis using a finite element method (FEM). For comparison, Type304 stainless steel was investigated as well. Though both Type304SS and candidate material were also hardened by ion irradiation, the increase in apparent hardness of the candidate material was smaller than that of Type304SS. The yield stress and uniform elongation were estimated from the calculated constitutive equation by FEM inverse analysis. The irradiation hardening of the candidate material by irradiation can be expected to be lower than that of Type304SS.

Keywords: High-chromium austenitic stainless steel, Cladding tube, LWR, Ultra high burnup, Ion irradiation, Constitutive equation, Finite element method, Hardness, Mechanical properties, Indentation test

1. Introduction

The ultra-high burnup of LWR is considered to be an important technology for establishing nuclear power plants as one of the most promising future energy system in point view of reducing radioactive wastes and electrical cost. Cladding materials with the excellent long performance under heavy irradiation would be required to these developments. The high chromium austenitic stainless steels(25Cr-35Ni-0.2Ti UHP)[1] were selected as one of candidates that is possible to made by the present engineering technologies. And, there are many practical irradiation data as fuel cladding tubes made of austenitic stainless steels in LWRs and LMFBRs. Many fuel cladding tubes made of austenitic stainless had been suffered

* Corresponding author, Tel:+81-29-282-6385 Fax:+81-29-282-6489.
E-mail adderess: ioka@popsvr.tokai.jaeri.go.jp (I.Ioka)

from environmental cracking along with longitudinal in early BWR and PWR plants[2-5]. Moreover, the uniform elongation of Type 304SS and 316SS was rapidly decreased with increasing neutron dose[6-8] at the practical temperature range (473-673K). Therefore, it is important to suppress environmental cracking and ductility loss on the high chromium austenitic alloys for cladding tubes. A triple ion beam facility at JAERI was used for simulating the effect of irradiation on the mechanical properties of the candidate material. However, the ion irradiated area is limited to the very shallow surface layer (<2μm depth) so that the irradiation damage is distributed around the thin layer. A indentation technique was applied to examine the ion irradiation effect on the mechanical properties of the thin layer[9].

In this study, the change in apparent hardness of the very shallow surface layer of the irradiated material was calculated from the slope of load/depth-depth curve which is in direct proportion to the appearance hardness of the material. Besides, the Swift's power low constitutive equation ($\sigma=A(\varepsilon_0+\varepsilon)^n$, A: strength coefficient, ε_0: equivalent strain by cold rolling, n: strain hardening exponent) of the damaged parts was derived from the microindentation test combined with an inverse analysis[10] using a finite element method (FEM). The material properties of the candidate material were compared with that of Type 304SS after ion irradiation to evaluate the irradiation hardening characteristics of the candidate material.

2. Experimental procedure

2.1 Material

The chemical composition of candidate material is 25Cr-35Ni-Ti UHP with high austenite stability at irradiation temperature as shown in Table I. It was melted using cold crucible induction melting (CCIM) for attaining ultra high purity of which total impurities is less than 100ppm. The billet was prepared by hot forging after solution annealed at 1373K for one hour and water cooled. The cladding tube with 11.3mm in outer diameter, 0.4mm in thickness and 1000mm in length was produced by incorporating the thermo-mechanical treatment so-called SAR (abbreviated the strained, aged and recrystallized)[11]. The treatment consists of 65% cold-worked, aged at 873K for 15hours and recrystallized at 1048K for 10hours. The interstitial solutes such as C, N, and O are stabilized in intra-grains as uniformly distributed fine precipitates. Finally, 7% cold-worked was conducted to the cladding tube for getting the sufficient tensile strength and for stretching. Type 304SS tubes were also used as a reference of stainless steel cladding tubes in the past commercial use of LWRs. The reference is the same Type 304SS cladding tubes made for fuel elements used in 'Mutsu'. The final thermal history is 8% cold-worked after solution annealed.

Table 1 Chemical Composition of the Material Tested in Weight Percent (%).

Materials	Fe	C	Si	Mn	P	S	Cr	Ni	Ti	N	O	Co
25Cr-35Ni-Ti UHP	bal.	0.0013	<0.005	0.001	0.001	0.0009	24.55	34.99	0.18	0.0014	0.0011	
Type 304SS	bal.	0.063	0.49	1.45	0.016	0.012	18.72	10.27				0.03

The specimens for ion irradiation were cut into 3mm diameter by the slurry drill from cladding tubes and then the bulge of the specimen was removed by polishing precisely. The surface of the specimen was finally electro-chemically polished. The specimens were irradiated using triple ion beam accelerator equipped in the TIARA at Takasaki site of JAERI. The irradiation condition was selected based on the condition calculated with computer simulation by assuming 100Gwd/t(MOX) on ABWRs. The dose rate, helium by (n, α) and hydrogen by (n, p) were adjusted by the ion irradiation of 12MeV Ni^{3+}, 1.1MeV He^+ and 380keV H^+ at 573K corresponding to cladding surface temperature. The Ni^{3+}, He^+, and H^+ ion beams were generated by Tandem accelerator, Single-ended accelerator and Ion implanter respectively. More detailed description of the triple ion beam facility is given elsewhere[12].

For triple ion beam irradiation, the beams were applied simultaneously. The Ni^{3+} ion produces displacement damage in the surface layer of the specimen. The He^{+} and H^{+} ions simulate the effect of He generation during Ni(n, α) and the effect of H generation during Ni(n, p), respectively.

The SRIM97 code was used to calculate the implanted ion distribution and the displacement dose as a function of depth from the specimen surface. The calculation results are shown in Fig.1. Fig.1(a) represents the displacement damage in dpa by Ni^{3+} as a function of depth from the surface. The displacement damage by He^{+} and H^{+} ions is disregarded, because they are small. The peak dose is about 110dpa around 2μm. The He^{+} and H^{+} ions were implanted in depth ranges from 1.0 to 1.5μm using energy degraders with aluminum foil. Fig.1(b) shows the distribution of the implanted Ni^{3+}, He^{+} and H^{+} ions in the specimen as a function of depth. The peak of Ni^{3+} ion (2.8at%) occurs about 2μm. The He^{+} and H^{+} ions in the implanted range were 100-150 appmHe and 1000-1600 appmH, respectively. The implanted He^{+} and H^{+} ions were controlled to neglect the effect of implanted Ni^{3+} ions. The ratios of helium and hydrogen concentrations to dpa (appm/dpa) were about 2-3 appmHe/dpa and 20-30 appmH/dpa for simulating 100Gwd/t(MOX) on ABWRs condition. The damage rate was about $1.6x10^{-3}$ dpa/s.

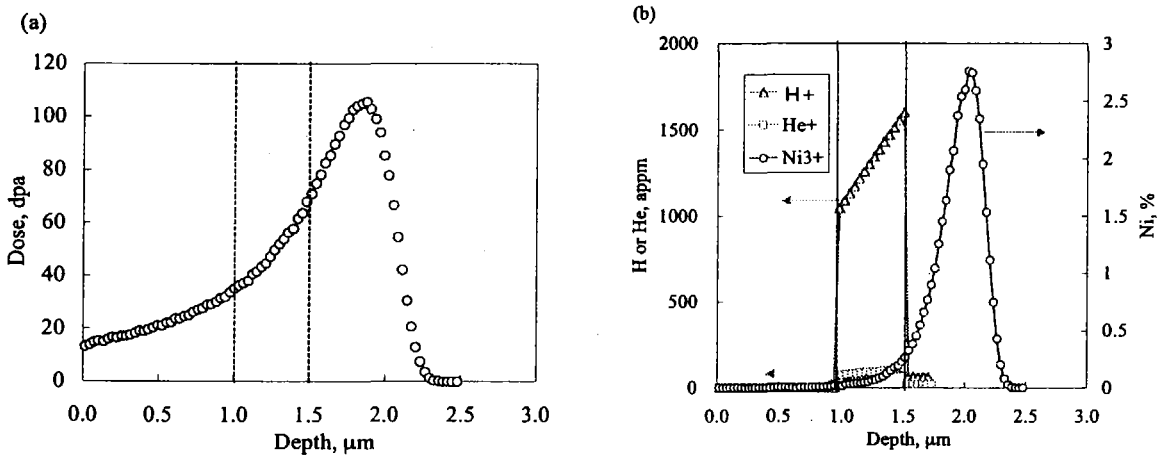

Fig.1 Depth profiles of (a) displacement damage by nickel and (b) nickel, hydrogen and helium concentrations in the specimen irradiated by triple beams

2.2 Indentation test

The indentation tests were carried out on the polished surfaces of specimens at room temperature. Two types of indenters were used for the indentation test. One is the Berkovich indenter for measuring the apparent hardness, the other is the conical indenter that has a hemispherical apex with radius of 1.2μm for deriving the constitutive equation. A testing machine, DUH-201 (Shimazu Co, Japan), was used for it. During loading and unloading, the load and indent depth were continuously measured with a resolution of 19.6μN and 1 nm, respectively. A load was imposed through the indenter on the specimen's surface with loading rate of 2.7mN/s, held for 1s, and then removed. The maximum load of 100mN was chosen not to be affected by the size effect manly due to the roughness of the indenter apex and the roughness of the specimen surface, as taking both the indentation depth and the radius of the indenter apex into account.

2.3 Identification of constitutive equation

The inverse analysis was carried out using an explicit FEM code, LS-DYNA, which

enables us to robustly analyze a large deformation accompanying with contacting behavior. In the analysis, the indenter and specimen were treated as axisymmetric two-dimensional bodies to take calculative efficiency into account. The modeled indenters were perfectly rigid. The contact interface between the specimen and the indenter was assumed to be frictionless, because the frictional force induced with friction coefficient up to 0.3 had few effects on the load-depth relationship. The mesh size is given to be sufficiently fine to keep accuracy: the minimum element size around the apex contacting zone was 0.05μm. The total number of the elements used in the model was 1509. The loading rate in the calculation was small enough to neglect an inertia effect as a static condition.

The constitutive equation of the material installed into the model was assumed to be a simple power-law which is generally believed to be applicable to normal metallic materials as follows:

$$\sigma = E\varepsilon \qquad \sigma \le \sigma_y \tag{1}$$

$$\sigma = A(\varepsilon_0 + \varepsilon)^n \tag{2}$$

$$\varepsilon_0 = (\sigma_y / A)^{1/n} - (\sigma_y / E) \qquad \sigma > \sigma_y \tag{3}$$

where, σ is true stress, ε true strain, E Young's modulus, σ_y yield stress, A work hardening coefficient and n work hardening exponent. Hereafter, we have to identify the following material constants; σ_y, A and n through the inverse analysis on the load-depth, L-D, curve.

The flow chart of the identification with inverse analysis is illustrated in Fig. 2. Here, **C** and **E** are determinants of material constants and estimated errors of material constants. **Z** and **Y** are determinants of experimental and calculated values on L and dL/dD. **R** is determinant of error in measuring systems. S_{max} is the maximum number of steps in the divided L-D curve. **H** is $\partial \mathbf{Y}/\partial \mathbf{C}$. The procedure of the inverse analysis is as follows.

1) $\mathbf{C_0}$, $\mathbf{E_0}$, **R** and S_{max} are input as initial values.
2) $\mathbf{Z_s}$ of L and dL/dD at step S is input.
3) $\mathbf{Y_s}$ of L and dL/dD at step S is calculated by FEM code.
4) The estimated values on **C** and **E** are given by the following equation of Kalman filter using each value, $\mathbf{C_s}$, $\mathbf{E_s}$, $\mathbf{Y_s}$, $\mathbf{H_s}$ and **R** at step S,

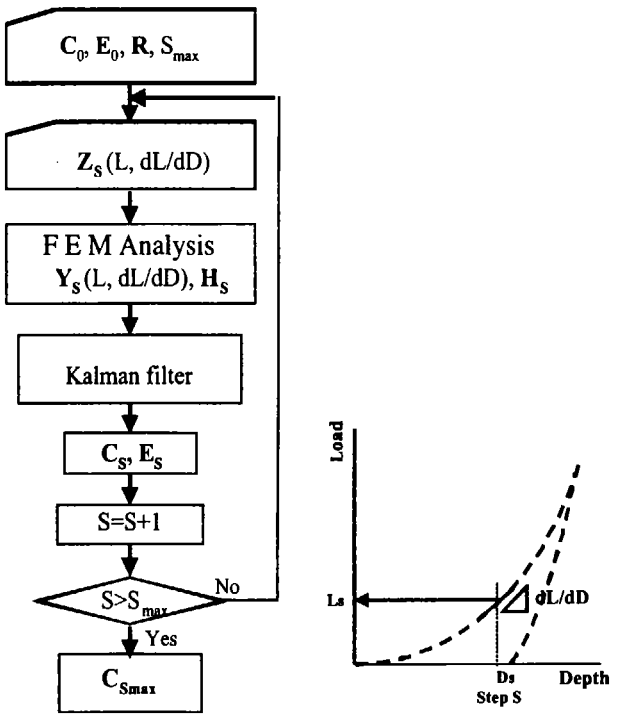

Fig.2 Flow chart for identification of material constants

$$\mathbf{C_S} = \mathbf{C_{S-1}} + \mathbf{E_S H_S R^{-1}}\left(\mathbf{Z_S} - \mathbf{Y_S}\right) \tag{4}$$

$$\mathbf{E_S} = \left(\mathbf{E_{S-1}}^{-1} + \mathbf{H_S}^{T}\mathbf{R^{-1}H_S}\right)^{-1} \tag{5}$$

5) Go back to 2) and repeat the process up to S_{max}. Finally we can obtain the optimal values C_{Smax} estimated at final step S_{max}.

3. Results and discussion

3.1 Hardness

The relationships between load and depth obtained by the indentation test of 25Cr-35Ni-Ti UHP and Type 304SS were expressed as the L/D-D curves, as shown in Fig.3. Each data point is an average from five indentations. The measured curves of the unirradiated(solid line) and triple ion irradiated(dotted line) specimens are plotted together. The curves were fitted with **L/D=a+bD**, where **D** is a depth (μm) from the surface, **L** is the load(gf) at that depth, and **a** and **b** are constant. In particular, the value of **b** is in direct proportion to the appearance hardness of the material[13]. The initial stage up to around 0.1μm in each curve should be neglected because this part of the curve is very dependent on surface roughness of the specimen and the roundness of indenter's tip shape, regardless of the change of the material property. The slope of the ion irradiated curve is higher than that of the unirradiated curve up to a depth of 0.4μm. It means that the ion irradiated layer (about 2μm) affects the L/D-D response of the ion irradiated specimen up to 0.4μm depth.

Figure 4 shows the relative ratio of appearance hardness for the irradiated specimens normalized to it of original specimens. The irradiation defects such as black dots, loops, and bubbles are considered to be strongly relation to the irradiation hardening and ductility loss. The irradiation hardening of 25Cr-35Ni-Ti UHP is expected to be lower than that of Type 304SS from fig.4.

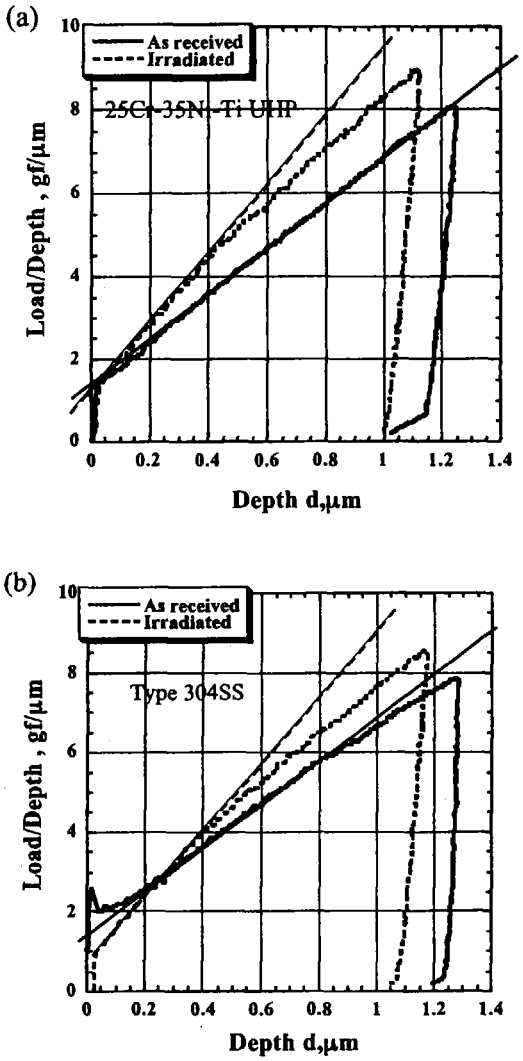

Fig.3 load/depth-depth (L/D-D) curves of 25Cr-35Ni-Ti UHP and type 304

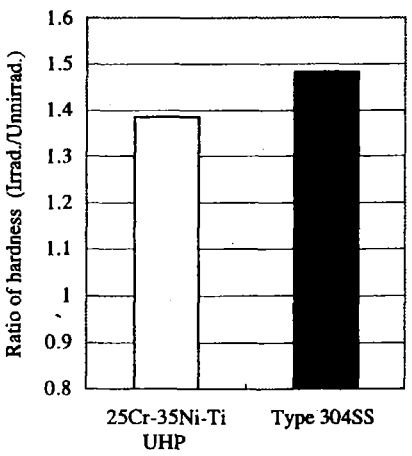

Fig.4 Relative ratio of hardness for specimens irradiated 50dpa by triple ion beams to it of original specimens at 278K

3.2 Constitutive equation

Figure 5 shows the L-D curves measured using the conical indenter, and the calculated results using material constants in Eqs (1)-(3) identified according to the method with the inverse

analysis on the L-D curve. Regardless of the materials, the calculated L-D curves agree with the experimental ones well. The material constants estimated from the inverse analyses on the L-D curves of 25Cr-35Ni-Ti UHP and Type 304SS are summarized Table 2. Increase in yield stress of Type 304SS was bigger than that of the 25Cr-35Ni-Ti UHP. It is well known that a hardness can be related to a yield stress. The result is in fairly good agreement with the change in apparent hardness as shown in Fig.4. The change in the value of A is same in both specimens by ion irradiation. The value of n corresponds to the uniform deformation of the material. After ion irradiation, the decrease in n of Type 304SS was bigger than that of 25Cr-35Ni-Ti UHP. So, it seems that the ductility loss of Type 304SS by ion irradiation is larger than that of 25Cr-35Ni-Ti UHP. As a result, the irradiation hardening of the candidate is expected to be lower than that of Type 304SS from Fig.4 and the estimated material constants.

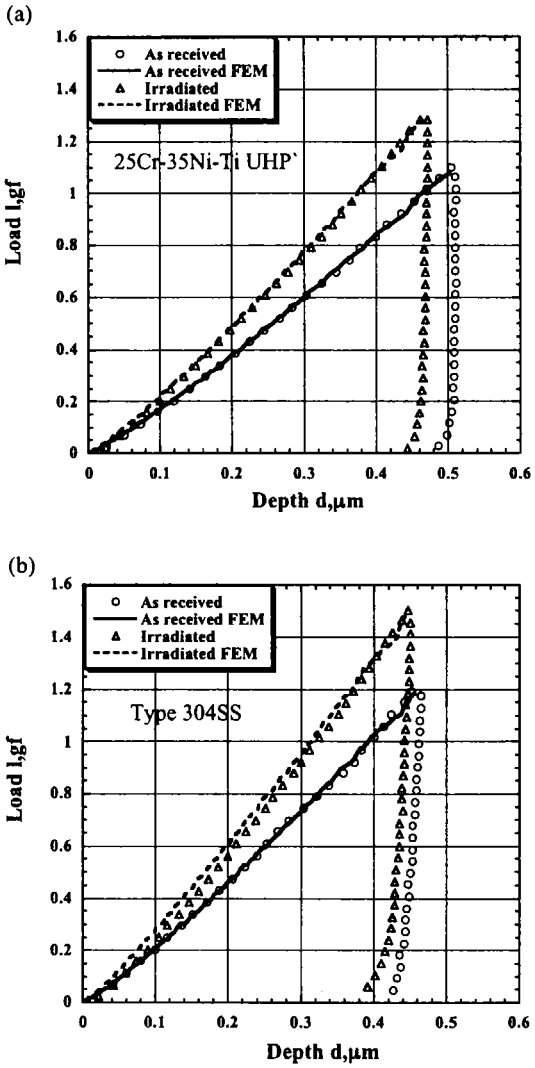

Fig.5 L-D curves measured using the conical indenter, and the calculated results by the inverse analysis

4. Conclusions

The mechanical properties of the ion irradiated material which is a candidate for ultra-high burnup fuel cladding was examined using the novel technology used the indentation technique combined with numerical calculation.

(1) The apparent hardness of Type 304SS was higher than that of the candidate after ion irradiation.

(2) The constants in the constitutive equation for the ion irradiated thin layer were determined by the inverse analyses with Kalman filter.

(3) The mechanical properties of the irradiated thin layer was deduced using the obtained constitutive equation.

(4) Increase in yield stress of Type 304SS was bigger than that of the candidate. The result is in fairly good agreement with the result of apparent hardness.

Table 2 The material constants estimated from the inverse analyses on the L-D curves of 25Cr-35Ni-Ti UHP and Type 304SS

		σ_y, MPa	A, MPa	n
Type 304SS	Unirrad.	213	1464	0.29
	Irrad.	528	1564	0.23
	Irrad./Unirrad.	2.45	1.07	0.79
25Cr-35Ni-Ti UHP	Unirrad.	191	1397	0.36
	Irrad.	411	1492	0.33
	Irrad./Unirrad.	2.15	1.07	0.92

Acknowledgements

The authors would like to thank Mr. K.Tachibana and T.Suzuki of JAERI for the experiment, and also thank to Dr. M.Fujiwara of KOBELCO Co. for preparation of the specimens.

References

[1] K.Kiuchi, I.Ioka, M.Takizawa, and S.Wada, "Development of Advanced Cladding Materials for Burnup Extension", IAEA TCM Reports on Technical and Economic Limit to Fuel Burnup Extension", Argentina(1999).

[2] T.J.Pashos, "Experience with Stainless Steel as a Fuel Clad Material in Water-Cooled Power Reactors," APED-4260(1963).R.DUCAN, "Stainless Steel Failure Investigation Program,"GEAP-5530(1968).

[3] I.Miller, "European Operating Experience," Joint Topical Meeting on Commercial Nuclear Fuel Technology Today," 75-CAN/ANS-100(1975).

[4] V.Pasupathi and P.Lingensmith, "Investigation of Stainless Steel Clad Fuel Rod Failures and Fuel Performance in Connecticut Yankee Reactor," EPRI NP-2119(1981).

[5] D.R.Harries, "Neutron Irradiation-Induced Embrittlement in Type 316 and Other Austenitic Steels and Alloys," Journal of Nuclear Materials, 82, 2(1979).

[6] M.L.Grossbeck, K.Ehrkich and C.Wassilew, "An Assessment of Tensile, Irradiation Creep, Creep Rupture and Fatigue Behavior in Austenitic Stainless Steels with Emphasis on Spectral Effects", Journal of Nuclear Materials, 174, 264(1990).

[7] J.P.Robertson, I.Ioka, A.F.Rowcliffe, M.L.Grossbeck and S.Jitsukawa, "Temperature Dependence of the Deformation Behavior of Type 316 Stainless Steel After Low Temperature Neutron Irradiation", Effects of Radiation on Materials: 18th International Symposium , ASTM STP 1325, 671, R.K.Nanstad,

[8] M.L.Hamilton, F.A.Garner and A.S.Kumar, Eds., American Society for Testing and Materials, West Conshohocken, PA, USA(1999).

[9] I.Ioka, M.Futakawa and T.Wakui, "Mechanical characterization on ion irradiated thin surface layer by nanoindentation technique with inverse analysis", 7th Inter. Conf. on Nucl. Eng., Tokyo, Apr.19-23, ICONE-7095(1999).

[10] M.Futakawa, T.Wakui, Ytanabe and I.Ioka, "Stress-Strain Relationship Evaluated by Inverse Analysis on Indentation Load-Depth Curve".

[11] K.Kiuchi, M.Kikuchi and K.Kondo, "A New Type of Low Temperature Sensitization of Austenitic Stainless Steels Enhanced with Defect-Solute Interactions", Journal of Nuclear Materials, 179-181, 481(1991).

[12] TIARA GROUPE, "JAERI TIARA Annual Report (1992); April 1991-March 1992, "JAERI-M-93-047(1993).

[13] H.Takahashi et al., "Development of evaluation techniques for small specimens", Atomic Energy Society of Japan, (1992)84.